Ultrasound in Medicine & Biology 49 (2023) 1852–1860

Contents lists available at ScienceDirect

Ultrasound in Medicine & Biology

journal homepage: www.elsevier.com/locate/ultrasmedbio

Original Contribution

Controlled Hyperthermia With High-Intensity Focused Ultrasound and Ultrasound Contrast Agent Microbubbles in Porcine Liver

Eric K. Juang [a], Lance H. De Koninck [a], Kaleb S. Vuong [a], Aswin Gnanaskandan [b], Chao-Tsung Hsiao [c], Michalakis A. Averkiou [a,*]

[a] Department of Bioengineering, University of Washington, Seattle, WA, USA
[b] Department of Mechanical and Materials Engineering, Worcester Polytechnic Institute, Worcester, MA, USA
[c] Dynaflow Inc., Jessup, MD, USA

ARTICLE INFO

Keywords:
Microbubbles
High-intensity focused ultrasound
Ultrasound contrast agents
Acoustic shadowing
Hyperthermia
Perfusion
Heated area
Thermal lesion

Objective: The objective of this work was to study microbubble-enhanced temperature elevation with high-intensity focused ultrasound (HIFU) at different acoustic pressures and under image guidance. The microbubbles were administered with either local or vascular injections (that mimic systemic injections) in perfused and non-perfused *ex vivo* porcine liver under ultrasound image guidance.

Methods: Porcine liver was insonified for 30 s with a single-element HIFU transducer (0.9 MHz, 0.413 ms, 82% duty cycle, focal pressures of 0.6–3.5 MPa). Contrast microbubbles were injected either locally or through the vasculature. A needle thermocouple at the focus measured temperature elevation. Diagnostic ultrasound (Philips iU22, C5-1 probe) guided placement of the thermocouple and delivery of microbubbles and monitored the procedure in real time.

Results: At lower acoustic pressures (0.6 and 1.2 MPa) in non-perfused liver, inertial cavitation of the injected microbubbles led to greater temperatures at the focus compared with HIFU-only treatments. At higher pressures (2.4 and 3.5 MPa) native inertial cavitation in the tissue (without injecting microbubbles) resulted in temperature elevations similar to those after injecting microbubbles. The heated area was larger when using microbubbles at all pressures. In the presence of perfusion, only local injections provided a sufficiently high concentration of microbubbles necessary for significant temperature enhancement.

Conclusion: Local injections of microbubbles provide a higher concentration of microbubbles in a smaller area, avoiding acoustic shadowing, and can lead to higher temperature elevation at lower pressures and increase the size of the heated area at all pressures.

Introduction

High-intensity focused ultrasound (HIFU) is an emerging therapeutic modality currently used for targeted ablation of benign tumors, such as uterine fibroids [1–3], and malignant tumors in the prostate [4–6], liver [7,8], kidney [9], pancreas [9,10] or bone [11]. The non-invasive nature of HIFU has also made it an attractive complement to conventional treatment options such as transarterial chemoembolization (TACE), where studies have reported improved short-term and long-term outcomes in patients with liver cancer when combining HIFU with TACE [12–18]. However, delivering sufficient acoustic energy through hard tissues (*e.g.,* skull or dense fibrous tissue) or anatomical barriers (*e.g.,* intra-abdominal fat) to the intended target has been a challenge that has prevented HIFU from being more widely applicable [19]. For instance, the use of magnetic resonance-guided HIFU for the treatment of essential tremor requires high acoustic intensities to overcome the amount of sound that is absorbed or reflected by the skull [20]. This increase in acoustic energy input may be complicated by unwanted heat deposition outside the focus or intended target, potentially leading to burns in the skin and subcutaneous fat [21]. Therefore, there exists a need for a method to elevate temperature locally with HIFU at lower acoustic intensities without causing significant collateral damage.

The difficulties associated with accurate energy deposition can be mitigated by administering microbubbles during HIFU, which are conventionally used as ultrasound contrast agents (UCAs). UCAs are clinically approved for use in cardiology applications, such as the assessment of coronary artery disease via left ventricular opacification in contrast echocardiography [22], and liver applications, such as the evaluation of liver masses in both adult and pediatric patients [23–25]. Although ultrasound imaging with UCAs, commonly known as contrast-enhanced ultrasound (CEUS), does not increase the temperature of the surrounding tissue, several studies have explored the potential of heating

* Corresponding author. Department of Bioengineering, University of Washington, Box 355061, N107 William H. Foege Building, 3720 15th Avenue NE, Seattle, WA 98195-5061, USA.
E-mail address: maverk@uw.edu (M.A. Averkiou).
Eric K. Juang and Lance H. De Koninck contributed equally to this work.

https://doi.org/10.1016/j.ultrasmedbio.2023.04.015
Received 30 November 2022; Revised 7 April 2023; Accepted 25 April 2023

enhancement when combining microbubbles (either exogenous UCAs or microbubbles generated *in situ* because of cavitation) with HIFU, which operates at much higher focal intensities than CEUS. Holt and Roy [26] investigated cavitation-enhanced heating at various acoustic pressure amplitudes and insonation durations in two types of tissue-mimicking phantoms (*i.e.,* polyvinyl alcohol and agar), using thermocouples to monitor temperature elevation at various distances away from the acoustic axis. Although they did not introduce UCAs in their work, they generated small bubbles in situ through acoustic cavitation and observed marked enhanced heating when the inertial cavitation threshold was exceeded. Later studies done by Tran et al. [27,28] revealed that UCA microbubbles injected during HIFU can act as cavitation nuclei and lower the energy threshold for HIFU-based thermal ablation. Tung et al. [29] studied bubble-enhanced heating by embedding Definity microbubbles of various concentrations in polyacrylamide phantoms. They reported a reduction in required energy input for a fixed temperature elevation and an increase in the size and a shift of the location (proximal to the transducer focus) of thermal lesions. Clark et al. [30] further investigated the concentration-dependent effect of microbubble-enhanced heating using egg white gel phantoms with diluted UCAs and real-time ultrasound imaging. They suggested that sustained microbubble cavitation by way of an optimal combination of acoustic pressure input and microbubble concentration is the key to effective ultrasound heating. Interestingly, at high concentrations the diluted UCAs, which are interspersed inside the egg white gel phantoms, introduced non-linear attenuation of pre-focal microbubbles that modified the HIFU pressure field through acoustic shadowing. These changes can make the temperature elevation and the location of thermal lesions unpredictable and complicate the use of HIFU. Administering microbubbles to a specific location in the phantom or tissue via local injection was suggested as a method to mitigate this issue, but it has not been investigated previously.

Although tissue-mimicking phantoms dosed with microbubbles offer a controlled environment to study HIFU, it is still a departure from the physiological environment of the human body where microbubbles travel with blood in the vasculature. The use of tissue models that are more representative of the human body, such as animal models or *ex vivo* perfused organs, is important for the study of HIFU-induced local hyperthermia. McDannold et al. [31] used contrast-enhanced magnetic resonance imaging to evaluate the effects of HIFU-microbubble combined heating and observed greater local energy absorption in rabbit brain tissue when compared with HIFU-only treatment. Yu et al. [32,33] reported higher rates of HIFU-induced necrosis in rabbit and goat liver models when microbubbles were used. Hanajiri et al. [34] treated induced tumors in rat livers with HIFU and Levovist (Schering, Berlin, Germany) microbubbles and reported significantly greater tissue coagulation in the HIFU−microbubble treatment group when compared with HIFU−saline treatment. Kaneko et al. [35] also observed similar effects in a rabbit liver model. However, the aforementioned studies have not investigated the effect of microbubble concentration coupled with the acoustic pressure or the method of microbubble delivery (dilution, vascular/systemic or local injections), and consequently, any advantages of controlled bubble-enhanced heating remain unknown.

The goal of this work was to quantitatively assess local hyperthermia when using HIFU and commercial UCA microbubbles concurrently in non-perfused porcine liver and *ex vivo* machine-perfused porcine liver [36,37]. The use of machine-perfused *ex vivo* porcine livers enabled us to study the effect of heat convection caused by blood flow and perfusion. Special emphasis was placed on microbubble concentration and the method of delivery in relation to the acoustic pressure. Vascular injections that mimic systemic *in vivo* injections and local injections were considered. We investigated the extent of focal temperature elevation in porcine liver tissues as a result of HIFU application, with and without microbubbles, at different acoustic pressures and a range of temperature elevations including mild hyperthermia. Ultrasound guidance via a clinical ultrasound scanner was used to direct HIFU to predetermined targets in the porcine liver tissue and align the thermocouple. Computer simulations were used to predict and validate the observed temperature elevation in perfused and non-perfused porcine liver when using HIFU alone.

Methods

Experimental setup

The experimental setup consisted of a porcine liver (preparation described in a later section) partially submerged in a container filled with either degassed, deionized water or blood mimicking fluid (perfusate) (Fig. 1). The liver was insonified from above using a single-element focused transducer (H116; Sonic Concepts, Bothell, WA, USA) operating at 0.9 MHz. The transducer was mounted on a metal cage and attached to a manual three-axis micropositioner (Newport Corp., Irvine, CA, USA). A custom 4-cm-long acrylic coupling cone (C-101; Sonic Concepts) filled with de-gassed water was fitted to the HIFU transducer to couple it to the liver. The end of the cone has a thin elastic membrane, which was coupled to the liver with ultrasound gel. The purpose of the cone was to provide an adjustable offset between the transducer's surface and the entry plane as the liver sample was thinner than the actual focal length. The cone provides a fixed distance of degassed water to guide ultrasound to the sample and avoid any form of cavitation before entering the liver. Ultrasound pulses were generated with an arbitrary function generator (AFG3102C; Tektronix, Beaverton, OR, USA) and amplified by a linear power amplifier (2200L; Electronics & Innovation, Rochester, NY, USA), before being transmitted by the transducer. HIFU was delivered as 372,000 cycle pulses fired at a pulse repetition frequency of 2 Hz (82% duty cycle) for 30 s. The 2 Hz frame rate was selected to allow for interleaving of the HIFU exposure as described by Clark et al. [30]. The focal acoustic pressures selected for our experiments were 0.63, 1.25, 2.50 and 3.75 MPa, as measured in water with a hydrophone. Each measurement was averaged 128 times, and the peak-to-peak amplitude divided by 2 was recorded as the amplitude. Because of non-linear propagation in the water, the peak positive and peak negative values for the aforementioned pressures were 0.67 and −0.59, 1.38 and −1.12, 3.0 and −2.0 and 4.81 and −2.69 MPa, respectively. The uncertainty of the membrane hydrophone was 13%. Taking into consideration the liver tissue attenuation, the *in situ* pressures in the liver were estimated to be 0.6, 1.2, 2.4 and 3.5 MPa. As it was not possible to measure the *in situ* pressures in the liver and most propagation takes place in the water-filled cone, we assume that the peak positive and negative values *in situ* would be analogous to those reported for water above. *In situ* pressures are used in the remainder of the article and the figures. A C5-1 curved array transducer connected to a Philips iU-22 scanner (Philips

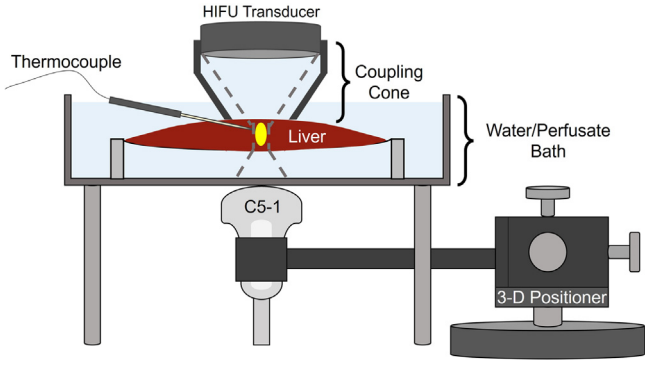

Figure 1. Experimental setup for high-intensity focused ultrasound (HIFU) treatment of *ex vivo* porcine liver. A three-axis micropositioner allows alignment of the imaging transducer (placed below the liver) with the HIFU transducer and thermocouple. A plastic cone filled with de-gassed water couples the transducer to the liver surface. The liver is submerged in perfusate liquid.

Healthcare, Bothell, WA, USA) was placed below the liver to provide real-time ultrasound images and to guide the placement of a thermocouple (MT-26/6HT; Physitemp Instruments, Clifton, NJ, USA), which is a needle microprobe. The needle thermocouple was positioned in the liver such that its tip was at the focus of the HIFU transducer. In addition to temperature measurements at the focus, we also measured the temperature at locations away from the focus by translating the HIFU transducer. The procedure for alignment of the needle thermocouple with the HIFU transducer and the imaging plane is further described below.

Acoustic pressure measurement

The transverse and axial pressure fields of the HIFU transducer were measured in an ultrasonic water tank with a 0.4-mm-sensor-diameter polyvinylidene fluoride membrane hydrophone (UT1604-225; Precision Acoustics, Dorchester, UK) calibrated in the range 1–30 MHz. Hydrophone measurements were compared with theoretical predictions based on the Rayleigh integral to find more accurate estimates of the transducer radius and focal length [30]. The focal depth and diameter were found to be 62.1 and 58.2 mm, respectively. The half-amplitude distances in the axial and transverse directions were ~15.8 and ~2.5 mm, respectively. We can model the focal volume as a prolate spheroid with the above half-amplitude distances as its semi-axes:

$$V = \frac{4}{3}\pi\left(\frac{R}{2}\right)^2\left(\frac{Z}{2}\right) \quad (1)$$

Here, R and Z are the transverse and axial half amplitude distances respectively, resulting in an estimated volume, V, of 51.71 mm^3. To evaluate the influence, if any, of the C-101 coupling cone on the acoustic field, hydrophone measurements at the focus were taken with and without the cone attached and no differences were noted. Also, because the acoustic impedances of water and liver tissue are very similar, the reflection coefficient is 0.02, suggesting very little, if any, energy reflecting at the interface.

Liver tissue preparation

The sources of porcine livers used in this work include local commercial farms, slaughterhouses and affiliated research groups that used porcine research models for other research purposes. Use of *ex vivo* perfused livers in this study did not require an Institutional Animal Care and Use Committee approval, as verified by our academic institution. Our machine-perfused porcine liver setup is a modified version of the procedure previously described [36,38]. Briefly, a porcine liver was resected from a deceased pig with the portal vein and the hepatic artery largely preserved. The resection was completed within 30 min of the animal's death to limit ischemic necrosis as well as stenotic and thrombotic changes to the hepatic tissue, which would otherwise severely compromise the *ex vivo* perfusion of the liver in the laboratory. Once the liver is outside the body, the portal vein and hepatic artery of the liver were cannulated and flushed, first with 8 L of lactated Ringer's solution (6 L at room temperature and 2 L ice-cold), then with 3 L of ice-cold histidine–tryptophan–ketoglutarate (HTK) solution (prepared in-house). Subsequently, the liver was submerged in 2 L of HTK solution in static cold storage and transported back to the laboratory, where it was connected to a normothermic machine-perfusion system. The liver was then perfused with 8 L of blood-mimicking fluid that consisted of Powdered Williams Medium E (Sigma-Aldrich, St. Louis, MO, USA), sodium bicarbonate (Sigma-Aldrich), heparin (Fisher Scientific, Waltham, MA, USA), insulin (Lantus SoloStar Pen, Sanofi, Paris, France) and dexamethasone (Sigma-Aldrich). The liver was also supplied with 95% oxygen/5% carbon dioxide via an oxygenator (Affinity NT Oxygenation System; Medtronic, Dublin, Ireland) in a custom-made machine-perfusion system to maintain the viability of the liver. Two flowmeters (EW-32461-44 and EW-32460-40, Cole-Parmer) were used to regulate perfusion to the portal venous system and hepatic arterial system. Finally, the liver was submerged in blood-mimicking fluid using the setup illustrated in Figure 1. For the non-perfused livers, we used untreated segments of the machine-perfused livers after they were removed from the machine-perfusion system.

Microbubble injection and temperature measurement

Alignment of the HIFU transducer and the needle thermocouple was done with ultrasound guidance by the method described by Keravnou et al. [38] (Fig. 2). First, the needle thermocouple was inserted into a 19G needle, which acted as a sound-reflective sheath for identifying the location of the thermocouple as well as a stationary channel for local injections. This thermocouple–needle combination was then inserted into the porcine liver and spatially manipulated until maximal echogenicity was visualized on the iU-22 ultrasound scanner (Fig. 2a). Visualization of the thermocouple–needle combination was possible because of incomplete linear signal cancellation in the non-linear amplitude modulation mode [39] of the imaging probe. The HIFU transducer with the coupling cone was then placed on the liver tissue from above, and the amplifier was activated while the function generator remained off. This produced a radiofrequency interference signal (Fig. 2b) in the ultrasound image where the focus of the HIFU beam could be visualized and aligned with the tip of the needle. The precision of the alignment technique is ±0.5 mm. Another option for aligning the thermocouple was the use of small temperature increases with low-amplitude exposures. However, this technique can still cause some microbubble disruption, and we opted not to use it.

Sonazoid microbubbles (GE Healthcare, Amersham, UK) were introduced to the liver via local injections with a 19G needle at the HIFU

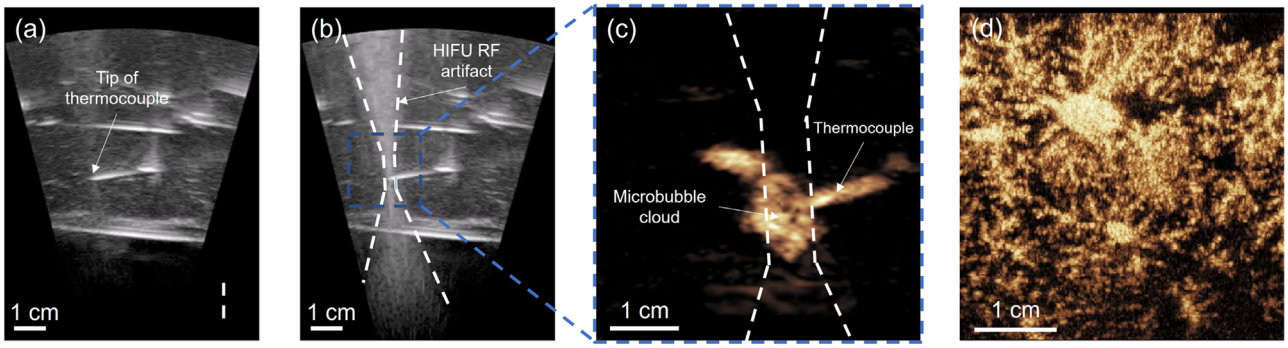

Figure 2. (a) B-mode (fundamental) image of the liver revealing placement of the thermocouple in the target area. (b) By use of a radiofrequency (RF) artifact, the focus of the high-intensity focused ultrasound (HIFU) transducer is shown in the liver image and aids the placement of the tip of the thermcouple at the focus. (c) Contrast image of the liver revealing microbubbles after a local injection collecting at the tip of the thermocouple. (d) Contrast image of the liver revealing the vessel structure of a liver area after a systemic microbubble injection in a perfused pig liver.

focus (which is also at the tip of the thermocouple as previously described) or vascular injections (mimicking systemic *in vivo* injections) into the portal vein and hepatic artery, also with a 19G needle and through an inline rubber port. When local injections of microbubbles were used, the thermocouple was briefly removed from the guide needle and 0.05 mL of Sonazoid (estimated concentration: 2×10^8 MBs/mL) was injected through the same guide needle directly into the tissue (not the vessels) using a method similar to that by which percutaneous ethanol injections are performed for clinically treating some liver tumors. The presence of the injected microbubbles was confirmed with the C5-1 imaging probe while scanning in contrast mode (Fig. 2c). Contrast images were collected using a non-linear technique (amplitude modulation at 1.7 MHz) at a low mechanical index (0.05) to avoid bubble destruction and in a contrast side-by-side format with non-linear imaging on one side and fundamental imaging on the other [39]. The thermocouple was immediately re-inserted through the guide needle after the bubble injection. Realignment was performed where necessary. When using vascular/systemic injections of microbubbles, simultaneous injections of 0.3 mL of Sonazoid into the portal vein and/or hepatic artery were performed. The microbubbles then flow to the area of interest with the blood flow in the same way that systemic intravenous injections arrive in the liver of patients. The time between injection of the microbubbles and arrival at the site of interest, as confirmed with contrast imaging (Fig. 2d), was about 30 s.

The sequences of HIFU application were identical regardless of local or vascular/systemic injection of the microbubbles. First, baseline temperature measurements at the HIFU focus were recorded prior to HIFU application. All experiments took place at room temperature, 23°C. Previous studies have reported that microbubble response at room temperature differs only slightly from responses at body temperature (37°C) and can be offset by using slightly higher concentrations [40]. After HIFU was switched on, focal temperature measurements were recorded. To make off-axis temperature measurements, the three-axis micropositioner was used to adjust the lateral position of the HIFU transducer while the thermocouple remained fixed.

Bioheat simulations

Temperature elevation is defined as $\Delta T = T - T_0$, where T and T_0 are the current and initial temperatures, respectively. In the absence of microbubbles, ΔT was modeled using the bioheat transfer equation described by Pennes [41]. The bioheat equation is a linear parabolic heat equation that assumes tissue can be modeled as a continuum, where heating effects from vessels are uniformly accounted for to avoid localized inhomogeneities. The equation addresses two mechanisms of heat transfer in the body—conduction within the tissue and convection caused by blood flow—and three methods of heat generation—absorption of energy, blood perfusion and metabolic activity. In the study described here, we used *ex vivo* tissue, so we ignored the metabolic energy term in the equation. To address both tissue types, we used the following bioheat equation to predict change in temperature per unit volume:

$$\rho c_p \frac{\partial T}{\partial t} = \kappa \nabla^2 T + Q + Q_p \tag{2}$$

where ρ is the density of the medium (water: 1000, liver: 1060 kg/m^3), c_p is the specific heat capacity of the medium (water: 4180, non-perfused liver: 3500 J/kg/K, perfused liver: 3500 J/kg/K), κ is the thermal conductivity of the medium (water: 0.610, liver: 0.534 W/m/K) and T represents temperature in degrees Kelvin (K). The final two terms, Q and Q_p, are the rate of heat generation from the acoustic field and the rate of heat transfer caused by blood perfusion per unit volume, respectively. For monochromatic sound waves, the rate of energy generation per unit volume in tissue can be expressed as

$$Q = 2\alpha I \tag{3}$$

where α is the absorption coefficient of the medium (water: 0.025, non-perfused liver: 8.19 Np/m/MHz, perfused liver: 4 Np/m/MHz), and I (Pa^2) is the intensity of the radiated waves. As this equation assumes monochromatic waves, it does not apply when there is non-linear propagation and harmonic generation. For the higher pressures used in the present work there may be some non-linear distortion that was not modeled with our theoretical simulations because we assumed monochromatic waves at the amplitudes that we have measured in water and then de-rated for tissue attenuation. The transfer of thermal energy from blood flow per unit volume is given as

$$Q_p = c_B W_B (T - T_B) \tag{4}$$

where c_B, W_B and T_B are the specific heat capacity (3770 J/kg/K), perfusion rate (kg/m^3/s) and ambient temperature (K) of blood respectively [42]. In this study, the perfusate solution flowing through the machine-perfused model mimics the properties of blood and was maintained at room temperature such that $T_B \sim 23$°C. As the rate of perfusion was limited by the flow rate of the machine-perfusion system, the perfusion rate was estimated from an average flow rate of 200 mL/min for 10 L of perfusate with density 1060 k/m^3 to yield $W_B = 0.3533$ kg/m^3/s. For modeling machine-perfused tissue, all terms are used to predict temperature, while for non-perfused modeling, $Q_p = 0$.

Results

Non-perfused ex vivo *tissue*

The measured change in focal temperature (ΔT) in non-perfused *ex vivo* liver tissue (N = 8) as a function of time for different pressures is illustrated in Figure 3. The *blue curves* represent the measured (*dashed line*) and simulated (*dotted line*) ΔT in the absence of microbubbles. The *green lines* represented ΔT when microbubbles are used. The *shaded regions* represent one standard deviation.

At low pressures, 0.6 MPa (Fig. 3a) and 1.2 MPa (Fig. 3b), with no microbubbles injected, there is a gradual temperature increase when HIFU is active from 10 s to 40 s, followed by a gradual temperature decrease as the liver tissue cools. Measurements and simulations are in good agreement at these low pressures. When microbubbles are introduced at these pressures, two prominent indicators of tissue heating are seen: an initial rapid temperature rise within the first second of HIFU activation, and a significant difference in peak temperature compared with HIFU-only treatments. At 0.6 MPa there was a 3.5°C increase in ΔT during the first second of heating and a 7°C difference in peak ΔT. The same trend with an initial 4.9°C ΔT increase during the first second of heating and a 12°C difference in peak ΔT was observed at 1.2 MPa. However, at higher pressures, 2.4 MPa (Fig. 3c) and 3.5 MPa (Fig. 3d), we see that the temperature profiles with or without microbubbles are similar. This result was assumed to be caused by cavitation of residual air micropockets in the liver tissue, an effect confirmed with imaging during the procedure. At these higher pressures, cavitation is nucleated in both cases, from either UCAs or trapped gas pockets in the tissue, and we observe similar ΔT regardless of whether microbubbles had been injected. For clarity, the shaded region representing a standard deviation has been removed from the higher pressures as error behavior was consistent with the corresponding shaded regions of the lower pressures. Simulations of HIFU with no microbubbles at these higher pressures (2.4 and 3.5 MPa) reveal a similar or slower temperature rise compared with our measurements. Interestingly, the cooling behavior at 3.5 MPa was much slower with microbubbles than without. One reason for this might be the irregular shape of the UCA bolus (see, *e.g.,* Fig. 2c), which may have caused the location of the maximum heating to take place slightly away from the tip of the thermocouple. The slow cooling may also be attributed to a larger area being heated and a longer time being required to cool down. These two points are discussed further in the next section.

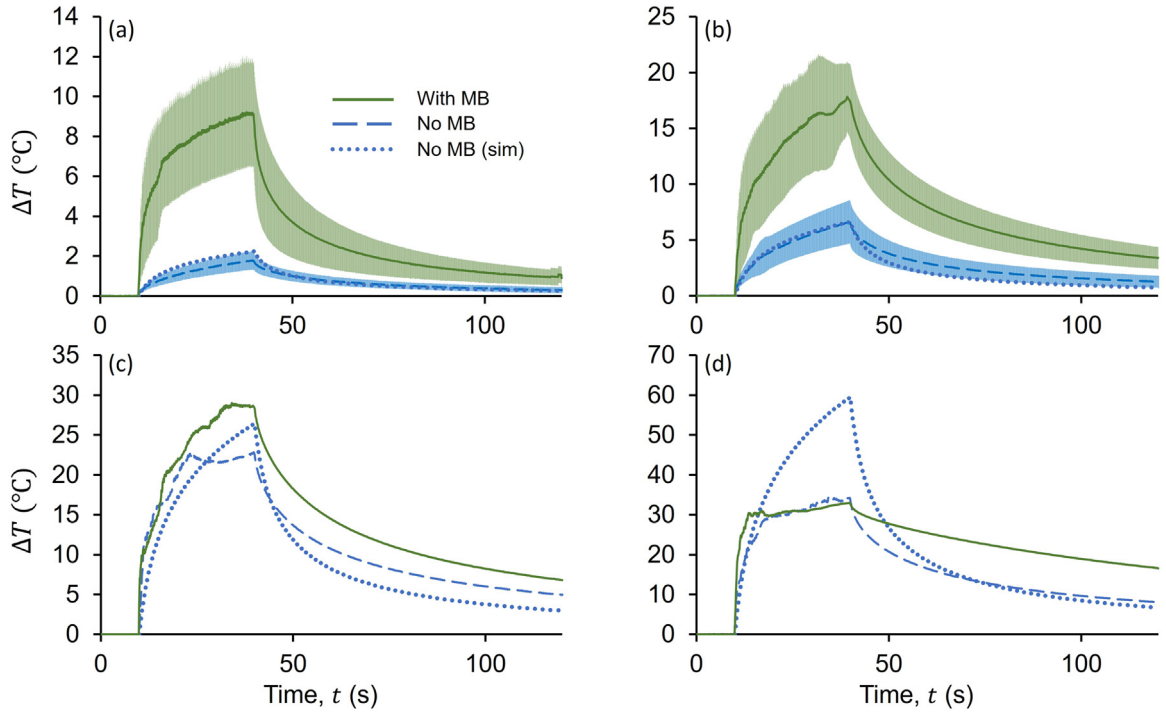

Figure 3. Measured and simulated temperature elevation (ΔT) with and without microbubbles during 30 s of high-intensity focused ultrasound (HIFU) exposure and 80 s after exposure at four focal acoustic pressures: (a) 0.6 MPa, (b) 1.2 MPa, (c) 2.4 MPa, (d) 3.55 MPa. *Shaded areas* indicate one standard deviation. MB, microbubbles; sim, simulation.

The ΔT for all pressures is further summarized in Figure 4a, which illustrates the peak measured focal ΔT at each non-derated (water) focal pressure in the presence and the absence of microbubbles. The temperature gain caused by microbubbles is the difference between the *green* (with bubbles) and the *blue* (without bubbles) lines. At lower pressures (0.6 and 1.2 MPa) there is a greater temperature gain, and at higher pressures this effect is reduced mainly because of cavitation in the tissue caused by air pockets and other native cavitation nuclei. At the highest pressure setting (3.5 MPa), the maximum ΔT was the same with and without microbubbles. Native cavitation also increased the variability of peak temperature measurements at higher pressures, represented by larger error bars at 2.4 and 3.5 MPa. Another time of interest was 35 s after heating had concluded (at 75 s total time according to Fig. 3) to investigate the cooling of the medium and is illustrated in Figure 4b. ΔT was consistently greater at this time point for all focal pressures when microbubbles were injected into the tissue (the *green line* is above the *blue line),* and it continued to increase with increasing focal pressure. Given the ΔT saturation observed in Figure 4a at 3.5 MPa and the increased retention of heat for all focal pressures with microbubbles in Figure 4b, heating with microbubbles leads to similar temperatures but slower cooling rates compared with HIFU alone, which in turn suggests a larger heated area has been formed at higher pressures (2.5 and 3.5 MPa). The heated area is defined as the area where the temperature during HIFU exposure is greater than half the maximum temperature reached. A positive outcome from using microbubbles is when the relative ΔT with injected microbubbles is greater than the ΔT without microbubbles and/or the heated area with microbubbles is greater than the heated area without microbubbles. The results for 3.5 MPa are further discussed in the next section.

In Figure 5, ΔT is illustrated with (*green*) and without (*blue dashed*) microbubbles measured 1 mm radially away from the axis at the focus for all the pressures considered. At this location, the measurements reveal significant ΔT enhancement when using microbubbles at all pressures. Native cavitation described above that reduced the temperature enhancement at the higher pressures on axis (Fig. 3c, 3d) is less pronounced off axis. To be able to clearly distinguish the differences between the curves, we did not include a shaded region representing a

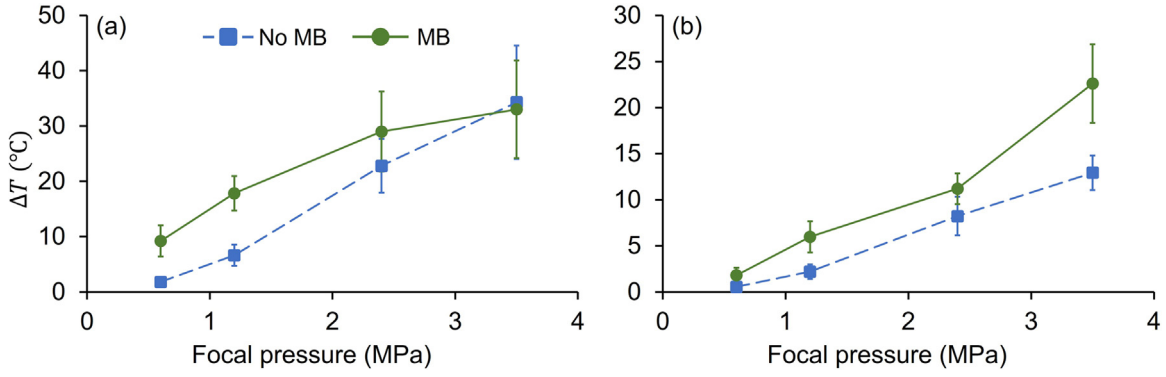

Figure 4. Measured temperature elevation as a function of acoustic pressure (a) after 30 s of heating and (b) 35 s after the end of heating. *Error bars* indicate one standard deviation. MB, microbubbles.

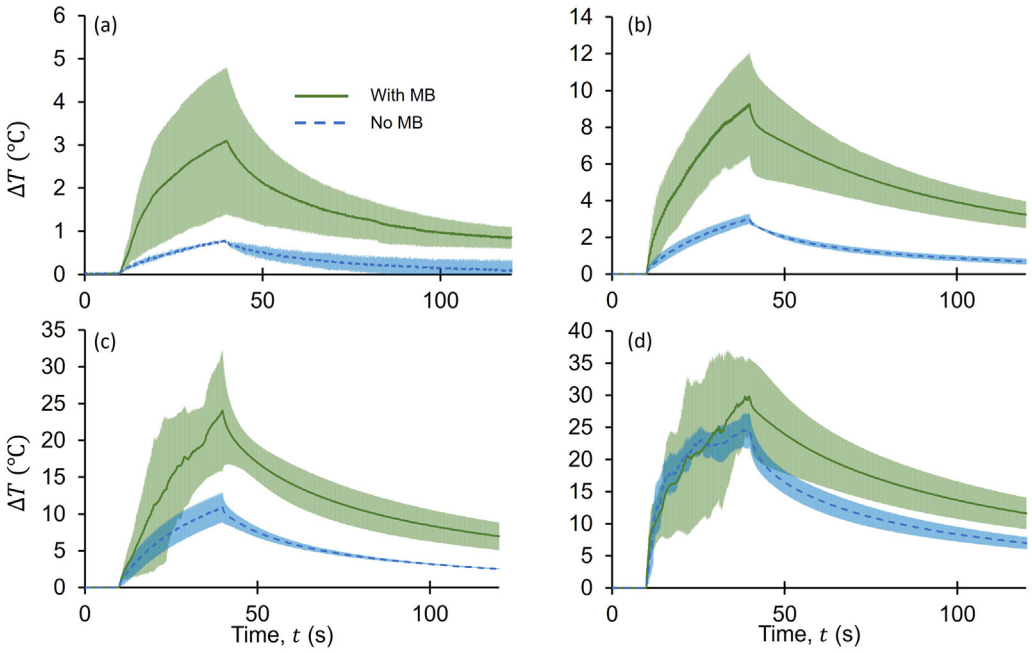

Figure 5. Measured temperature elevation 1 mm radially off axis with and without microbubbles for four non-derated focal pressures: (a) 0.6 MPa, (b) 1.2 MPa, (c) 2.4 MPa, (d) 3.5 MPa. *Shaded areas* indicate one standard deviation. MB, microbubbles.

standard deviation. The recorded standard deviation was similar to that of the axial measurements in Figures 3 and 4.

Machine-perfused tissue

In Figure 6, ΔT measurements and predictions from eqn (2) in both perfused and non-perfused liver when not using microbubbles at an acoustic pressure of 1.2 MPa are shown to evaluate the effect of blood flow and perfusion. Measurements were repeated six times, and the *shaded area* represents the standard deviation (spread of our measurements). The use of machine perfusion (physiological flow in the liver) adds convection because of the flow, also modeled by eqn (2). For the same acoustic input energy, ΔT in the machine-perfused liver was lower compared with that in the non-perfused liver. Tissue cooling was faster in machine-perfused liver once HIFU was turned off. Heat was dissipated by the circulating perfusate, which acted as a heat sink because of its larger volume and lower relative temperature. Our simulations with perfusion mostly agree with the measured data but predict a faster cooling rate, which may indicate a reduced quality of expected perfusion in the *ex vivo* experiments.

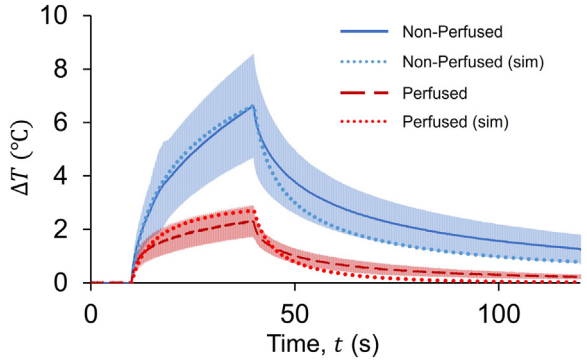

Figure 6. Focal temperature elevation (ΔT) in perfused and non-perfused porcine liver with no microbubbles at an acoustic pressure of 1.2 MPa (non-derated). *Solid and dashed lines* represent average measured temperatures of perfused and non-perfused liver respectively, with a *shaded region* indicating one standard deviation. The *dotted lines* represent predicted focal temperatures in perfused and non-perfused liver with no microbubbles. sim, simulation.

In Figure 7, we show ΔT in a perfused liver (N = 4) with and without microbubbles supplied either systemically (injected into the main feeding vessels) or locally (injected directly at the focus under image guidance) at pressures 1.2 MPa (Fig. 7a) and 2.4 MPa (Fig. 7b). Again, the shaded areas have been removed for clarity, with error trends with and without microbubbles established in Figures 3 and 6, respectively. A prediction of ΔT in the perfused liver without microbubbles (*dotted red line*) was also included for both pressures. At the lowest pressure (0.6 MPa, not shown here), there was no ΔT because of perfusion-related heat dissipation. At the highest pressure (3.5 MPa, also not shown here), intense cavitation activity confirmed with imaging resulted in no ΔT difference between using and not using microbubbles. At pressures 1.2 MPa (Fig. 7a) and 2.4 MPa (Fig. 7b), we observe that the local injections result in markedly higher ΔT as seen previously with the non-perfused liver. Vascular/systemic injections led to ΔT values similar to those observed without microbubbles at both pressures. Like the non-perfused liver temperature measurements in Figure 3, local injections in Figure 7 show a temperature profile at 1.2 MPa with a steep initial slope followed by a smooth temperature increase. At 2.4 MPa, the local injection temperature profile has an even steeper initial slope followed by temperature saturation caused by excessive cavitation. In summary, at these pressures there is a significant heating enhancement only with local injections.

Discussion

The objective of this work was to investigate temperature elevation with HIFU (noting that HIFU does not always imply thermal ablation) in the presence of UCA microbubbles in an *ex vivo* porcine liver, with and without machine perfusion, which we consider to be very close to the physiologic environment in human tissue. The use of machine perfusion allowed for evaluation of the effect of blood flow and perfusion on heat transfer in the liver. We compared HIFU with local microbubble injections at the focal region to HIFU with vascular/systemic microbubble injections via the portal vein and/or hepatic artery in terms of the tissue ΔT they induce. Heating enhancement was confirmed with needle thermocouple measurements (a) at the focus and 1 mm laterally away from

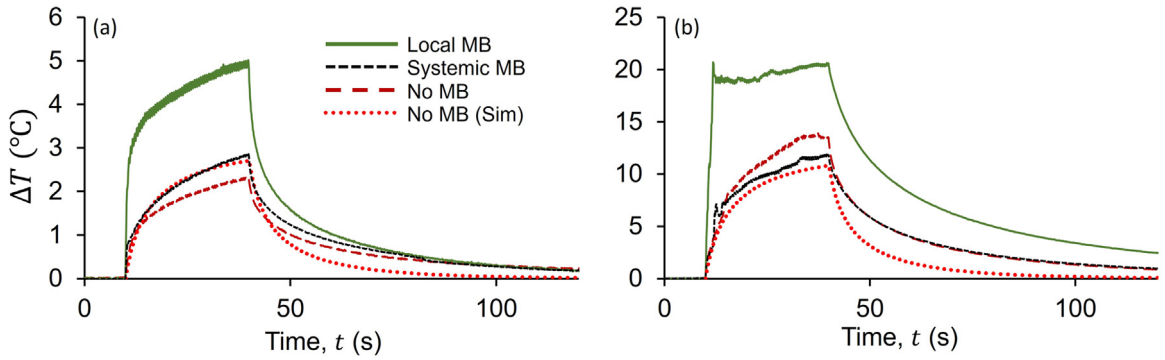

Figure 7. Measured focal temperature elevation (ΔT) in machine-perfused porcine liver with and without microbubbles (MB) at two focal pressures: (a) 1.2 MPa, (b) 2.4 MPa. Two microbubble delivery methods were used: local injection (*solid line*) and systemic injection (*short-dash line*). Theoretical predictions of focal temperature elevation in perfused porcine with no microbubbles are represented by *dotted lines*. MB, microbubbles; sim, simulation.

the focus after 30 s of heating and (b) 35 s after turning off HIFU and while the tissue was cooling down.

Our results indicated that, in both perfused and non-perfused porcine livers, HIFU with local microbubble injections led to greater tissue temperature elevation (ΔT) relative to HIFU-only treatment. In contrast, HIFU with systemic microbubble injections caused little to no enhancement in tissue temperature elevation compared with HIFU without microbubbles. We attribute this result to a need for a high concentration of microbubbles at the target area of the HIFU treatment but not everywhere else in the path of the beam. Clark et al. [30] reported a similar observation. They varied the concentration of uniformly diluted microbubbles in an egg white phantom and studied its effects on temperature elevation and lesion formation after HIFU exposure. They found that as the microbubble concentration increased, the heating enhancement from microbubbles also increased. However, as the microbubbles were evenly diluted throughout the phantom, their highest microbubble concentrations led to excess attenuation (acoustic shadowing) along the path of ultrasound. This shadowing shifted the maximum temperature and the treatment area away from their thermocouple and closer to the HIFU transducer. They used both optical images and pre-focal temperature measurements to confirm the shift of the heated area. In our study, local injections of microbubbles provided sufficient concentration only around the focal area and led to significant heating enhancement without encountering acoustic shadowing and the shift of the heated area observed by Clark et al. [30], as there are no microbubbles along the HIFU beam path to attenuate the sound. In our study, although vascular/systemic injections used a larger initial concentration of microbubbles compared with local injections, these microbubbles were diluted and distributed throughout the porcine liver vasculatures, resulting in low effective microbubble concentrations at the treatment site. In addition, the quality of perfusion in the *ex vivo* livers was moderate, and some areas were not fully perfused. Compromised perfusion in some tissue areas further reduced the number of available microbubbles for heating enhancement when using systemic injections. We suspect that these are the most prominent factors that led to the lack of enhanced tissue temperature elevation in HIFU with systemic microbubble injections. Although it may still be possible to enhance the heating with systemic injections of microbubbles in a more perfused tissue, we suspect that the higher concentrations of microbubbles will introduce acoustic shadowing as it was also observed in a previous study [30]. As such, we hypothesize that, to enhance heat deposition with HIFU with systemic administration of microbubbles, a fine balance must be struck between delivering sufficient microbubbles to the treatment site while preventing acoustic shadowing. An added complication is that the acoustic shadowing caused by high microbubble concentration is also amplitude dependent [43,44].

Our experimental results indicated that the acoustic pressure amplitude plays an important role. The ΔT increase at the focus resulting from the use of microbubbles was more pronounced at the two lower pressures (0.6 and 1.2 MPa) than at the two higher pressures (2.4-3.5 MPa). However, there was overall heating enhancement at all pressures as confirmed with the focal temperatures during the cooling process (Fig. 4b) and the off-axis measurements (Fig. 5), which also suggest an increase in the heated area. The increased cavitation activity around the focus (with injected UCAs or caused by native cavitation in tissue at higher pressures) can scatter the ultrasound in the neighboring tissue and increase the heated area.

We attribute the heating enhancement caused by microbubbles to two kinds of cavitation activity: cavitation of the injected UCA microbubbles and native cavitation within the medium without injecting microbubbles. Keller et al. [45] have previously studied cavitation of microbubbles, specifically the inertial cavitation threshold (evidenced by the onset of broadband noise in scattered frequency spectrum) of various clinical microbubbles. For Sonazoid, which we used in the present study, they found its cavitation threshold to be approximately 0.3 MPa in a water tank in which microbubbles were able to freely move. We suspect that in a physiological environment such as our porcine liver models, where Sonazoid microbubbles are spatially confined, the cavitation threshold is likely to be at a higher acoustic pressure. Using Sonazoid diluted in egg white gel phantoms, Clark et al. [30] found that sustained microbubble activity, which was assumed to be inertial cavitation, occurred above a critical pressure threshold of 0.5 MPa. Given the similar HIFU source and acoustic pressures, we can assume that the cavitation of microbubbles observed in this work was inertial at all focal pressures (0.6−3.5 MPa). Holt and Roy [26] studied native cavitation with microbubbles generated *in situ* in agar phantoms and found that surpassing the inertial cavitation threshold of these media led to enhanced focal temperatures. For longer pulse durations like the 30 s heating of this study, they found an inertial cavitation threshold of ~2 MPa, considerably larger than the threshold of clinical microbubbles. At these pressure settings, temperature measurements deviate from the bioheat equation when cavitation is not included in the model and exhibit a greater heating rate. Holt and Roy also noted a saturation of peak temperature as acoustic pressure increased beyond the inertial cavitation threshold, which they attributed to bubbles shielding the focal area by scattering the acoustic wave and diffusing energy deposition. Although we did not directly measure inertial cavitation in this study, our temperature elevation measurements and the points raised above suggest that inertial cavitation was likely present in all the conditions evaluated. Specifically, the temperature measurements for higher focal pressures (2.4 and 3.5 MPa) in the absence of UCA microbubbles (Fig. 3c, 3d), where both pressure settings led to temperature saturation and a similar or greater heating rate in the experiment compared with what simulations predicted, suggesting that inertial cavitation of the residual air micropockets and other cavitation nuclei within the liver occurs. Therefore, when UCA microbubbles are present, the two lower pressures (0.6 and

1.2 MPa) are above the inertial cavitation range of the UCA microbubbles but below the inertial cavitation threshold of residual air pockets in the medium. We refer to this pressure range as "controlled" bubble-enhanced heating. This is illustrated in Figure 4a for 0.6 and 1.2 MPa, where cavitation of the UCA microbubbles leads to significant ΔT enhancement. However, as pressure increases (*e.g.,* 2.4 and 3.5 MPa) beyond the inertial cavitation threshold of both the injected UCA microbubbles and residual air micropockets in the medium, intense cavitation shields the focal area from further energy deposition and ΔT reaches a plateau. We refer to this pressure range as "uncontrolled" bubble-enhanced heating. There is still some added benefit from using UCA microbubbles even at these higher pressures evidenced by the tissue temperature during cooling (Fig. 4b) and the off-axis measurements (Fig. 5).

One main limitation of this work was the accuracy of our needle thermocouple alignment, especially with microbubbles present. Another thermocouple-related limitation was that we were only able to measure the temperature at one point in space at a time. Although done under image guidance, the needle thermocouple was inserted by hand and had an estimated placement accuracy of 0.5 mm. The inaccuracy in placement is due largely to microbubbles obscuring the tip of the thermocouple, as seen in Figure 2c. As our thermocouple was initially aligned to the focus of the HIFU transducer, re-insertion of the thermocouple tip following microbubble injection may have caused it to shift away from the presumed HIFU focus per alignment. The irregular bolus shape of the microbubble cloud in Figure 2c may have also resulted in the ΔT saturation (*green line* plateaus at 3.5 MPa in Fig. 3d). At this high pressure, the microbubble cloud shape caused the maximum temperature elevation to occur slightly in front of the thermocouple. Thus, the actual maximum temperature in the tissue would likely have been much higher than 70° C and this would explain the much slower cooling rate observed. Given our setup, it was also not possible to align our thermocouple parallel to the acoustic axis (to limit the viscous heating artifact), as suggested by Holt and Roy [26] and also discussed in depth by Morris et al. [46]. As stated in the Morris et al. work, needle thermocouples (the type of thermocouple we used) generate a less viscous heating artifact or there is a second systematic effect, likely to be thermal conduction along the wire, which acts to reduce the effect of this heating. Also, our temperature measurements without microbubbles were in good agreement with our simulations, indicating that the viscous heating artifact did not significantly affect our measurements. Yet another limitation to our study is the use of only one thermocouple to take temperature measurements, which compromised our ability to directly probe the full size of the heated area created. This could be alleviated by using volumetric temperature measurement techniques such as thermal camera imaging [47] and magnetic resonance temperature measurements [48]. However, these potential workarounds introduce new challenges such as thermal imaging being limited to surface measurements and magnetic resonance having lower spatial and temporal resolution, in addition to being very costly and introducing compatibility complexities. Despite the aforementioned limitations to using a thermocouple, our approach proved to be simple and effective and to provide reliable temperature elevation measurements in tissue in the presence of microbubbles.

The clinical applicability of our findings is left to be determined because of the reliance on local injections of microbubbles as a means of enhancing temperature rise in a small target area. Although local injections are not a clinically approved method for UCA administration (only intravenous injections, which we have been referring to as systemic, are allowed), there have been research works reported in which *in vivo* local microbubble injections were used [49].

It still seems possible that systemic injections can significantly enhance the heating during HIFU *in vivo* only if an adequately high concentration of microbubbles is successfully delivered to the target area. Treatment of hypervascular tumors (not only for ablation but also for mild hyperthermia for enhanced drug delivery) may be a suitable target application for microbubble-enhanced HIFU. One example is hepatocellular carcinoma, which is a primary liver malignancy characterized by an early hypervascular arterial enhancement relative to the normal liver parenchyma in CEUS scans [50]. This could indicate an early diversion of blood flow to the tumor, which would increase microbubble concentration in the tumor and enhance heating during HIFU. Pending further investigation, a possibility remains that the microbubble concentration *in vivo* would not reach the optimal level required for significant heating enhancement with HIFU. The option to perform local bubble injections in a manner similar to that used to perform percutaneous ethanol injections clinically is still available and, according to the work presented here, might lead to more efficient local heating. Although *in vivo* work presents many new challenges, the insights into microbubble-enhanced heating from our work here may provide useful initial guidance toward the development and success of such treatments.

The methods proposed in the present work are not specifically targeted to HIFU ablation; they could be also used for drug uptake enhancement with local mild hyperthermia where a temperature elevation of 5°C–10°C is required. This would allow for a larger treatment area and transducers with lower focusing gains operating at lower amplitudes than HIFU ablation. Ultrasound cavitation treatments for enhanced drug delivery [38,51] that use long ultrasound pulses could be modified to deliver higher intensities (not necessarily amplitudes) and thus combine mechanical and thermal effects for treating the tumor microenvironment. We envision such a technique to be performed with either a few intravenous boluses or multiple small local injections of microbubbles and the treatment procedure to last 10-20 min. It may also be possible that a clinical imaging transducer could generate these conditions.

Conclusion

In this study we found that adjunctive use of HIFU with UCA microbubbles can lead to greater temperature elevations compared with HIFU alone. We identified the acoustic pressure and the microbubble concentration as the two important parameters. In non-perfused porcine liver, low acoustic pressures (<2 MPa) with local injections of microbubbles led to greater temperature elevation at the focus than when no microbubbles were used. Higher pressures (>2 MPa) produced cavitation in the tissue even without injecting microbubbles and offered reduced gain in focal temperature elevation when injecting microbubbles. At all pressures, the heated area was larger when microbubbles were injected.

In the perfused porcine liver where blood flow affects heat dissipation, we observed that only local injections of microbubbles had a sufficient microbubble concentration to induce enhanced heating during HIFU. There is a threshold microbubble concentration required for enhanced heating that the systemic injections were unable to provide. Overall, local injections of microbubbles can induce temperature increase and heated area enhancement in HIFU treatments.

Acknowledgments

The research reported in this study was supported by National Institutes of Health Grants 2R44CA213866-02 and 1R01EB032655-01A1. We also gratefully acknowledge that Sonazoid was supplied by GE Healthcare, Amersham, UK.

Conflict of interest

The authors declare no competing interests.

Data availability statement

The data used for this work can be made available on request.

References

[1] Kim HS, Baik JH, Pham LD, Jacobs MA. MR-guided high-intensity focused ultrasound treatment for symptomatic uterine leiomyomata: long-term outcomes. Acad Radiol 2011;18:970–6.

[2] Mahmoud MZ, Alkhorayef M, Alzimami KS, Aljuhani MS, Sulieman A. High-intensity focused ultrasound (HIFU) in uterine fibroid treatment: review study. Pol J Radiol 2014;79:384–90.

[3] Verpalen IM, de Boer JP, Linstra M, Pol RLI, Nijholt IM, Moonen CTW, et al. The Focused Ultrasound Myoma Outcome Study (FUMOS): a retrospective cohort study on long-term outcomes of MR-HIFU therapy. Eur Radiol 2020;30:2473–82.

[4] Poissonnier L, Chapelon JY, Rouvière O, Curiel L, Bouvier R, Martin X, et al. Control of prostate cancer by transrectal HIFU in 227 patients. Eur Urol 2007;51:381–7.

[5] Crouzet S, Murat FJ, Pasticier G, Cassier P, Chapelon JY, Gelet A. High intensity focused ultrasound (HIFU) for prostate cancer: current clinical status, outcomes and future perspectives. Int J Hyperthermia 2010;26:796–803.

[6] Stabile A, Orczyk C, Hosking-Jervis F, Giganti F, Arya M, Hindley RG, et al. Medium-term oncological outcomes in a large cohort of men treated with either focal or hemi-ablation using high-intensity focused ultrasonography for primary localized prostate cancer. BJU Int 2019;124:431–40.

[7] Li CX, Xu GL, Jiang ZY, Li JJ, Luo GY, Shan HB, et al. Analysis of clinical effect of high-intensity focused ultrasound on liver cancer. World J Gastroenterol 2004;10:2201.

[8] Kennedy J, Wu F, Ter Haar G, Gleeson F, Phillips R, Middleton M, et al. High-intensity focused ultrasound for the treatment of liver tumours. Ultrasonics 2004;42:931–5.

[9] Wu F, Wang ZB, Chen WZ, Zou JZ, Bai J, Zhu H, et al. Extracorporeal focused ultrasound surgery for treatment of human solid carcinomas: early Chinese clinical experience. Ultrasound Med Biol 2004;30:245–60.

[10] Khokhlova TD, Hwang JH. HIFU for Palliative Treatment of Pancreatic Cancer. In: Escoffre J-M, Bouakaz A, editors. Therapeutic Ultrasound. Cham: Springer International Publishing; 2016. p. 83–95.

[11] Chen W, Zhu H, Zhang L, Li K, Su H, Jin C, et al. Primary bone malignancy: effective treatment with high-intensity focused ultrasound ablation. Radiology 2010;255 (3):967.

[12] Wu F, Wang ZB, Chen WZ, Zou JZ, Bai J, Zhu H, et al. Advanced hepatocellular carcinoma: treatment with high-intensity focused ultrasound ablation combined with transcatheter arterial embolization. Radiology 2005;235:659–67.

[13] Li C, Zhang W, Zhang R, Zhang L, Wu P, Zhang F. Therapeutic effects and prognostic factors in high-intensity focused ultrasound combined with chemoembolisation for larger hepatocellular carcinoma. Eur J Cancer 2010;46:2513–21.

[14] Jin C, Zhu H, Wang Z, Wu F, Chen W, Li K, et al. High-intensity focused ultrasound combined with transarterial chemoembolization for unresectable hepatocellular carcinoma: long-term follow-up and clinical analysis. Eur J Radiol 2011;80:662–9.

[15] Xu G, Luo G, He L, Li J, Shan H, Zhang R, et al. Follow-up of high-intensity focused ultrasound treatment for patients with hepatocellular carcinoma. Ultrasound Med Biol 2011;37:1993–9.

[16] Cui L, Liu XX, Jiang Y, Wu XJ, Liu JJ, Zhou XR, et al. Comparative study on transcatheter arterial chemoembolization, portal vein embolization and high intensity focused ultrasound sequential therapy for patients. Asian Pacific J Cancer Prev 2012;13:6257–61.

[17] Kim J, Chung D, Jung S, Cho S, Hahn S, Lee J. Therapeutic effect of high-intensity focused ultrasound combined with transarterial chemoembolisation for hepatocellular carcinoma <5 cm: comparison with transarterial chemoembolisation monotherapy—preliminary observations. Br J Radiol 2012;85:e940–6.

[18] Chok KS, Cheung TT, Lo RC, Chu FS, Tsang SH, Chan AC, et al. Pilot study of high-intensity focused ultrasound ablation as a bridging therapy for hepatocellular carcinoma patients wait-listed for liver transplantation. Liver Transpl 2014;20:912–21.

[19] Illing R, Kennedy J, Wu F, Ter Haar G, Protheroe A, Friend P, et al. The safety and feasibility of extracorporeal high-intensity focused ultrasound (HIFU) for the treatment of liver and kidney tumours in a Western population. Br J Cancer 2005;93:890–5.

[20] Rohani M, Fasano A. Focused ultrasound for essential tremor: review of the evidence and discussion of current hurdles. Tremor Other Hyperkinet Mov (NY) 2017;7:462.

[21] Mougenot C, Köhler M, Enholm J, Quesson B, Moonen C. Quantification of near-field heating during volumetric MR-HIFU ablation. Med Phys 2011;38:272–82.

[22] Mulvagh SL, DeMaria AN, Feinstein SB, Burns PN, Kaul S, Miller JG, et al. Contrast echocardiography: current and future applications. J Am Soc Echocardiogr 2000;13:331–42.

[23] Kono Y, Moriyasu F, Mine Y, Nada T, Kamiyama N, Suginoshita Y, et al. Gray-scale second harmonic imaging of the liver with galactose-based microbubbles. Invest Radiol 1997;32:120–5.

[24] Wilson SR, Burns PN, Muradali D, Wilson JA, Lai X. Harmonic hepatic US with microbubble contrast agent: initial experience showing improved characterization of hemangioma, hepatocellular carcinoma, and metastasis. Radiology 2000;215:153–61.

[25] Darge K, Papadopoulou F, Ntoulia A, Bulas DI, Coley BD, Fordham LA, et al. Safety of contrast-enhanced ultrasound in children for non-cardiac applications: a review by the Society for Pediatric Radiology (SPR) and the International Contrast Ultrasound Society (ICUS). Pediatr Radiol 2013;43:1063–73.

[26] Holt RG, Roy RA. Measurements of bubble-enhanced heating from focused, MHz-frequency ultrasound in a tissue-mimicking material. Ultrasound Med Biol 2001;27:1399–412.

[27] Tran BC, Jongbum S, Hall TL, Fowlkes JB, Cain CA. Microbubble-enhanced cavitation for noninvasive ultrasound surgery. IEEE Trans Ultrason Ferroelectr Freq Control 2003;50:1296–304.

[28] Tran BC, Jongbum S, Hall TL, Fowlkes JB, Cain CA. Effects of contrast agent infusion rates on thresholds for tissue damage produced by single exposures of high-intensity ultrasound. IEEE Trans Ultrason Ferroelectr Freq Control 2005;52:1121–30.

[29] Tung YS, Liu HL, Wu CC, Ju KC, Chen WS, Lin WL. Contrast-agent-enhanced ultrasound thermal ablation. Ultrasound Med Biol 2006;32:1103–10.

[30] Clark A, Bonilla S, Suo D, Shapira Y, Averkiou M. Microbubble-enhanced heating: exploring the effect of microbubble concentration and pressure amplitude on high-intensity focused ultrasound treatments. Ultrasound Med Biol 2021;47:2296–309.

[31] McDannold NJ, Vykhodtseva NI, Hynynen K. Microbubble contrast agent with focused ultrasound to create brain lesions at low power levels: MR imaging and histologic study in rabbits. Radiology 2006;241:95–106.

[32] Yu T, Fan X, Xiong S, Hu K, Wang Z. Microbubbles assist goat liver ablation by high intensity focused ultrasound. Eur Radiol 2006;16:1557–63.

[33] Yu T, Xiong S, Mason TJ, Wang Z. The use of a microbubble agent to enhance rabbit liver destruction using high intensity focused ultrasound. Ultrason Sonochem 2006;13:143–9.

[34] Hanajiri K, Maruyama T, Kaneko Y, Mitsui H, Watanabe S, Sata M, et al. Microbubble-induced increase in ablation of liver tumors by high-intensity focused ultrasound. Hepatol Res 2006;36:308–14.

[35] Kaneko Y, Maruyama T, Takegami K, Watanabe T, Mitsui H, Hanajiri K, et al. Use of a microbubble agent to increase the effects of high intensity focused ultrasound on liver tissue. Eur Radiol 2005;15:1415–20.

[36] Izamis ML, Efstathiades A, Keravnou C, Leen EL, Averkiou MA. Dynamic contrast-enhanced ultrasound of slaughterhouse porcine livers in machine perfusion. Ultrasound Med Biol 2014;40:2217–30.

[37] Izamis ML, Efstathiades A, Keravnou C, Georgiadou S, Martins PN, Averkiou MA. Effects of air embolism size and location on porcine hepatic microcirculation in machine perfusion. Liver Transpl 2014;20:601–11.

[38] Keravnou CP, De Cock I, Lentacker I, Izamis ML, Averkiou MA. Microvascular injury and perfusion changes induced by ultrasound and microbubbles in a machine-perfused pig liver. Ultrasound Med Biol 2016;42:2676–86.

[39] Averkiou MA, Bruce MF, Powers JE, Sheeran PS, Burns PN. Imaging methods for ultrasound contrast agents. Ultrasound Med Biol 2020;46:498–517.

[40] Mulvana H, Stride E, Tang M, Hajnal JV, Eckersley R. Temperature-dependent differences in the nonlinear acoustic behavior of ultrasound contrast agents revealed by high-speed imaging and bulk acoustics. Ultrasound Med Biol 2011;37:1509–17.

[41] Pennes HH. Analysis of tissue and arterial blood temperatures in the resting human forearm. J Appl Physiol 1948;1:93–122.

[42] Drizdal T, Togni P, Visek L, Vrba J. Comparison of constant and temperature dependent blood perfusion in temperature prediction for superficial hyperthermia. Radioengineering 2010;19:281–9.

[43] Keller S, Bruce M, Averkiou MA. Ultrasound imaging of microbubble activity during sonoporation pulse sequences. Ultrasound Med Biol 2019;45:833–45.

[44] Matsumoto Y, Allen JS, Yoshizawa S, Ikeda T, Kaneko Y. Medical ultrasound with microbubbles. Exp Thermal Fluid Sci 2005;29:255–65.

[45] Keller SB, Sheeran PS, Averkiou MA. Cavitation therapy monitoring of commercial microbubbles with a clinical scanner. IEEE Trans Ultrason Ferroelectr Freq Control 2020;68:1144–54.

[46] Morris H, Rivens I, Shaw A, Haar GT. Investigation of the viscous heating artefact arising from the use of thermocouples in a focused ultrasound field. Phys Med Biol 2008;53:4759.

[47] Song C, Marshall B, McLean D, Frank T, Cuschieri A, Campbell P, et al. Thermographic investigation of the heating effect of high intensity focused ultrasound. Conf Proc IEEE Eng Med Biol Soc 2005;2005:3456–8.

[48] Quesson B, de Zwart JA, Moonen CTW. Magnetic resonance temperature imaging for guidance of thermotherapy. J Magn Reson Imaging 2000;12:525–33.

[49] Qiu L, Zhang L, Wang L, Jiang Y, Luo Y, Peng Y, et al. Ultrasound-targeted microbubble destruction enhances naked plasmid DNA transfection in rabbit Achilles tendons in vivo. Gene Ther 2012;19:703–10.

[50] Wilson SR, Burns PN, Kono Y. Contrast-enhanced ultrasound of focal liver masses: a success story. Ultrasound Med Biol 2020;46:1059–70.

[51] Keller SB, Suo D, Wang YN, Kenerson H, Yeung RS, Averkiou MA. Image-guided treatment of primary liver cancer in mice leads to vascular disruption and increased drug penetration. Front Pharmacol 2020;11:584344.